Font-Pérez, A.; Soriano Martinez, L.; Pinheiro, SMDM.; Tashima, MM.; Monzó Balbuena, JM.; Borrachero Rosado, MV.; Paya Bernabeu, JJ. (2020). Design and properties of 100% waste-based ternary alkali-activated mortars: blastfurnace slag, olive-stone biomass ash and rice husk ash. Journal of Cleaner Production. 243:1-11. https://doi.org/10.1016/j.jclepro.2019.118568

DESIGN AND PROPERTIES OF 100% WASTE-BASED TERNARY ALKALI-ACTIVATED MORTARS: BLAST FURNACE SLAG, OLIVE-STONE BIOMASS ASH AND RICE HUSK ASH

Alba Font [(1)], Lourdes Soriano [(1)], Sayonara Maria de Moraes Pinheiro [(2)], Mauro M. Tashima [(3)], José Monzó [(1)], Maria Victoria Borrachero [(1)], Jordi Payá [(1)].

[(1)] ICITECH – GIQUIMA Group – Grupo de Investigación en Química de los Materiales de Construcción, Instituto de Ciencia y Tecnología del Hormigón, Universitat Politècnica de Valencia, Valencia, Spain.

[(2)] UFES - Federal University of Espírito Santo, Department of Civil Engineering, Brazil

[(3)] Universidade Estadual Paulista (UNESP), Faculdade de Engenharia de Ilha Solteira. MAC – Grupo de Pesquisa em Materiais Alternativos de Construção, Ilha Solteira-SP, Brazil.

Abstract

Alkali-activated cements (AACs) technology is being widely investigated as a replacement for ordinary Portland cement (OPC) for environmental benefits. Blast furnace slag (BFS) is one of the most well known precursors used in AACs, having comparable properties to those of traditional OPC-based materials. AACs require alkali solutions, which are commonly based on a combination of sodium or potassium hydroxides with sodium or potassium silicates in high concentration. These alkali solutions represent the use of chemical reagents, and thus can have major environmental, health and economic impacts. Olive-stone (also known as olive pits) biomass ash (OBA) is a residue mainly composed of calcium and potassium oxides. Rice husk ash (RHA) is a rich silica residue from the combustion of rice husk. The combination of both residues can produce a good activating reagent for BFS-based AACs. In the present work, 100% waste-based ternary alkali-activated mortars (TAAM) based on BFS activated by OBA and RHA were developed. The mortars were assessed in terms of their dosage, curing treatment and time evolution. Finally an eco-friendly 100% waste-based TAAM with 67.39 ± 0.44 MPa after 90 days of curing at 20ºC is obtained and a complete microstructural characterization shows a dense and compact matrix with binding gel products labelled as C(K)-S(A)-H and C(K)-S-H.

Keywords: Alkali-activated cement, blast furnace slag, olive-stone biomass ash, rice husk ash, ternary binder.

Abbreviations:

AACs: Alkali-activated cements

BAAMs: Binary alkali-activated mortars

TAAMs: Ternary alkali-activated mortars

TAAPs: Ternary alkali-activated cements

BFS: Blast furnace slag

OBA: Olive-stone biomass ash

RHA: Rice husk ash

1. Introduction

The relationship between climate change and human activity is evident. In the last century, global warming has been the reason for great natural catastrophes. Greenhouse gas emissions, especially from burning fossil fuels, are the main causes of this global warming.

The cement industry is responsible for 5–8% of the anthropogenic CO_2 emissions around the world (Andrew, 2018; Turner and Collins, 2013) and, according to some estimates, it could reach 12–23% in 2050 ("World busines council for sustainable development," n.d.). The use of alternative fuels, biomass and supplementary materials in the construction industry does not seem sufficient to reduce the CO_2 emissions: thus, taking into account the binder content and the associated CO_2 emissions of concrete respect to developed strength, Yang et al (2015) concluded that the value of the CO_2 emission intensity decreased strongly when the replacement level of clinker by supplementary cementing materials was increased up to 15–20%, and higher replacement values represented a large decrease on compressive strength beyond decreased CO_2 emission intensity. Hence, studies and investigations focusing on new ecological and sustainable materials are crucial to reduce environmental problems associated with this massive industry.

Nowadays, one of the great challenges in the construction industry focuses on the use of alkali-activated cements (AACs) or geopolymers. These binders can be produced without Portland cement. They are composed of two main components: an aluminosilicate material (named "precursor", usually derived from waste materials) and an alkaline activating solution (Shirley and Black, 2011). The alkaline activating solution (usually composed of alkali hydroxides, such as NaOH or KOH, and alkali silicates) allows the dissolution of the precursor and its subsequent polymerization in order to form the different structures responsible for the mechanical AACs performance.

According to the literature, the CO_2 emissions associated with the AACs production can be 55–75% lower than those obtained for Portland cement. Most of these emissions are produced by the activating solution, especially when sodium or potassium silicates are employed. Concretely, the 70–90% of total emissions from AACs production are associated to the activating solution (Mellado et al., 2014; Passuello et al., 2017; Yang et al., 2013).

For this reason, the replacement of commercial products by environmentally friendly activating solutions could achieve a significant reduction in the CO_2 emissions associated with AACs. In recent years, researchers have been making efforts to replace synthetic (commercial chemicals) alkaline silicates by alternative silica sources. In such case, the alkaline solution is composed of NaOH/KOH solution and an amorphous silica source. The main silica sources are rice husk ash (RHA), diatomaceous earth residues (DE), glass waste, sugar cane straw ash (SCSA) and silica fume (SF), among others (Font et al., 2018; Payá et al., 2017).

Several studies have been reported on the use of rice husk ash (RHA) as a source of silica (Bernal et al., 2015; Bouzón et al., 2014; Mejía et al., 2013). Bouzón et al. (2014) prepared mixtures of RHA, water and sodium hydroxide and they applied a reflux process (between 15 and 240 minutes) to achieve the alternative activating solution. The activation of the fluid catalytic cracking catalyst residue (FCC) with this alternative solution achieved mortars with 41 MPa compressive strength in only one day of curing

at 65ºC. These values resulted similar than the obtained by the control FCC samples activated with an equivalent mixture of NaOH and waterglass.

Mejía et al. (2016) studied two alternative sources of silica (RHA and DE) in metakaolin/fly ash (MK/FA) mixtures and they demonstrated that the strength of systems with the alternative silicate achieved 50% lower compressive strength than the commercial sodium silicate.

Torres-Carrasco and Puertas (2015) described a similar preparation to obtain the activating solution. They mixed waste glass and NaOH for 6 hours at 80 ± 2 º C and then the mixture was filtered. The filtered activating reagent was combined in different proportions with fly ash (FA) as precursor. The solutions based on NaOH 10M + waterglass and NaOH 10M + waste glass were compared: mortars activated with the alternative alkali solution system yielded, after 28 days of curing, similar compressive strength than in the case where commercial waterglass was employed.

Tchakouté et al. (2016) studied MK geopolymers with different activating systems by reacting NaOH with RHA or waste glass. They prepared the activator at 100ºC for 2 hours. After this time, the dissolution was filtered and the liquid was stored for one week before use. The presence of calcium in the sodium silicate derived from waste glass enhances the depolymerization of metakaolin particles and the results are slightly better than those obtained using sodium silicate from RHA.

Sugar cane straw ash (SCSA) can also be used as a silica source. Moraes et al. (2018) prepared different activating solutions by means of a thermal bottle and fabricated mortars using blast furnace slag as precursor. The authors analysed the influence of the time of reaction inside the thermal bottle and the influence of the SiO_2/Na_2O ratio (ε). The results demonstrated that the compressive strength values obtained were similar to those reached for RHA and less than the mixtures with the commercial reagent.

In the last few years, greener alternative alkaline activators have been investigated. In these cases, a total absence of commercial chemical reagents is achieved. Two types of activators have been reported: materials from industrial processes and those from agro-industrial processes. The wastes from industrial processes are rich in sodium compounds and the agro-industrial wastes usually contain potassium compounds. One example of industrial waste is Bayer liquor, which is produced form industrial manufacture of alumina in the Bayer process. Van Riessen et al. (2013) used this waste in mixtures with FA, and concluded that the mortars with this waste had similar strength to the reference mortar. Hu et al. (2018) investigated the use of red mud, another toxic residue from the Bayer process, as a partial precursor in fly ash geopolymers activated with sodium hydroxide and sodium silicate. The authors concluded that the high alkalinity of the red mud improve the geopolymerization but additional NaOH and waterglass was needed to achieve optimum compressive strength development. Recently, the reusing of red mud after their use in a flue gas desulfurization process (FGD) (Nie et al., 2019) as alternative activator was investigated. The activation of class C fly ash based mortars was assessed obtaining 30.3 MPa when the sulphate rich red mud (RMD) was employed as alkali source. With the use of RMD, 25% increase in strength was obtained compared to the geopolymer prepared with the original red mud. Another waste studied is the caustic solution waste from the industrial cleaning process of aluminium. This residue was used as activator in mixtures with FA (Fernández-Jiménez et al., 2017; Shirley and Black, 2011): a compressive strength similar to that obtained by mixtures activated with 8M NaOH was achieved.

Cheah et al. (2015) studied a high calcium wood ash (HCWA) obtained from the use of wood ash biomass. The resulting ash had CaO as a principal oxide (61%) and a smaller proportion of K_2O (12%). Different ratios of HCWA/FA were prepared and mixed with water. The mixtures achieved near to 18 MPa and the main reaction product was a potassium aluminosilicate hydrate (K-A-S-H) gel. Other hydration products formed in this reaction were tobermorite and hydrated gehlenite.

In the group of agro-industrial wastes, different biomass ashes were studied. Peys et al. (2016) studied rich potassium biomass ashes. The authors prepared geopolymers with metakaolin (MK) as precursor and biomass ashes as alkaline activator. Maize salt and maize cob ashes reached around pH=13 after mixing with water and yielded the best mechanical behaviour (30 MPa) after 2 days of curing at 80ºC.

Recently, Font et al. (2017) employed olive-stone (also known as olive pits) biomass ash (OBA) in mixtures with blast furnace slag (BFS) and compared these with mixtures with only water and with a 4M KOH solution. After 3 and 7 days of curing at 65ºC, the mixtures with OBA showed the best mechanical behaviour. At 7 days of curing, the mortar with OBA yielded a compressive strength of 30 MPa. The study of OBA as activator was extended with more percentages of substitution/addition in mortars with BFS by de Moraes Pinheiro et al. (2018). The mortars with the replacement of BFS by OBA yielded more than 20% higher compressive strength than the BFS-KOH systems. A compressive strength of 38 MPa was achieved when OBA was used as mineral addition (25%) for a BFS AAC system. The authors reported a comparison of OBA and kephalite (inert mineral addition) in order to distinguish the filler effect versus the chemical reaction of geopolymerization. The study concluded that the filler effect due the presence of OBA was negligible in terms of the mechanical behaviour.

In the present work, new 100% waste-based ternary alkali-activated mortars (TAAMs) are designed and investigated, where no commercial reagents need to be employed. An alternative potassium silicate solution based on a mixture of olive-stone biomass ash (OBA), rice husk ash (RHA) and water is developed for blast furnace slag (BFS) activation and the mechanical and microstructural properties of these alkali-activated materials are assessed.

2. Experimental procedure

2.1. Materials

The raw materials used in this work were an industrial by-product, blast furnace slag (BFS), and two agro-industrial residues: olive-stone (or olive pits) biomass ash (OBA) and rice husk ash (RHA).

BFS was used as a precursor in all mixtures. It was supplied by Cementval (Puerto de Sagunto, Valencia, Spain) and it has a 26.0 μm mean particle diameter (D[4,3]) and 17.3 μm median particle diameter (D50) after being ground in a ball mill. The olive stone biomass ash (OBA) was supplied by Almazara Candela (olive-oil company, Elche, Spain), where the resulting ash from the olive- stone combustion was collected from the bottom of the furnace. For employing the OBA in the alkali-activated system, it was necessary to grind it in a ball mill, resulting in a powder with a D[4,3] = 27.3 μm and D50 = 20.8μm (de Moraes Pinheiro et al., 2018). The rice husk ash (RHA) was supplied by DACSA S.A. (Tabernes Blanques, Spain). For the use of this ash as an alternative silica source in the activating solution, it was ground in a ball mill, resulting in a D[4,3] = 20.3 μm and D50 = 10.5μm.

The chemical compositions (XRF) of these three raw materials are summarized in Table 1 (Bouzón et al., 2014; de Moraes Pinheiro et al., 2018). The BFS is mainly composed of calcium oxide (40.15%) and silica (30.53%). The chemical analysis corroborated the alkaline nature of OBA, potassium (32.12%) and calcium (27.77%) oxides being the main components. Finally, for RHA it can be seen that the main composition is silica (85.58%).

Table 1
Chemical composition (XRF) of the raw materials.

Material	Oxide composition (wt%)										
	SiO_2	CaO	Al_2O_3	Fe_2O_3	Na_2O	MgO	K_2O	P_2O_5	SO_3	Others	LOI*
BFS	30.53	40.15	10.55	1.29	0.87	7.43	0.57	0.26	1.93	0.89	5.53
OBA	5.33	27.77	0.70	3.45	0.78	5.13	32.12	2.68	1.67	0.95	18.90
RHA	85.58	1.83	0.25	0.21	-	0.50	3.39	0.67	0.26	0.32	6.99

*Loss on ignition

2.2. Methods

The methodology applied for ternary systems (TAAMs) composed of BFS/OBA/RHA comprised the analysis of the mechanical properties and microstructural characteristics obtained in mortars and pastes. It is well known that the mechanical behaviour of alkali-activated BFS depends on the slag specific surface, curing temperature, activator concentration, and the nature of the alkaline activator (Wang et al., 1995). Thus, the study is divided into two main steps with two sub-studies for each step.

The amount of RHA was constant in the two steps (step 1 and step 2) and the difference between steps was the OBA/BFS mass ratio: i) in step 1, the OBA was used as addition (A) with respect to the precursor (OBA addition system); and ii) in step 2, the OBA was used as both an addition (A) and a replacement (R) with respect to the precursor (OBA addition plus replacement system).

The samples of TAAMs in step 1 were assessed in terms of their OBA addition content (sub-study 1.1) and curing temperature (sub-study 1.2). The TAAMs developed in step 2 were assessed in terms of the curing process (sub-study 2.1) and curing time (sub-study 2.2). The samples are named as follows:

- Sub-study 1.1: xA-B, where "x" is the % of OBA addition ("A") in mass respect the BFS. "B" is referring to the curing treatment (B – 65ºC,).
- Sub-study 1.2: 20A-y, where "y" is the curing treatment (B – 65ºC; C – 20ºC/100% RH; and M = 24h B + 6d C).
- Sub-study 2.1: 20A/20R-y, where OBA is used as addition (A) and replacement material (R) and "y" is the curing treatment as the previous step (sub-study 1.2).
- Sub-study 2.2: 20A/20R-Cz, where all samples were cured at room temperature (C – 20ºC/100% RH) and z is the test time evaluation (3, 7, 28, 60 and 90 days).

The designed mixes and the acronyms employed are summarized in Table 2.

The alkaline solutions were prepared 24 hours before the preparation of mortars, by means of sealed plastic bottles to improve the dissolution rate of the particles of both ashes. The corresponding OBA quantity (addition or addition/replacement) was dry mixed with RHA followed by the addition of water. The plastic bottles were sealed with a cap and kept in a thermal bath (65ºC). For the first 6 hours, the bottles were

manually shaken for one minute per hour, and were then left without agitation until the mortar was prepared. After this, the water suspensions were left at room temperature for one hour. Manufacture of the mortars consisted of mixing the precursor (BFS) with the corresponding activating solution for 60 seconds, and then addition of the sand to the obtained paste and stirring of the mixture for 180 seconds.

Table 2
TAAMs designed and studied distributed in each work step, with dosages by mass.

			Alkaline activator			Precursor	Precursor /sand
		Sample	H_2O (g)	OBA (g)	RHA (g)	BFS (g)	
Step 1	Sub-study 1.1	15A-B	202.5	67.5	40.0	450.0	1/3
		20A-B		90.0			
		25A-B		112.5			
	Sub-study 1.2	20A-B		90.0			
		20A-C					
		20A-M					
Step 2	Sub-study 2.1	20A/20R-B		180.0		360.0	1/3.75
		20A/20R-C					
		20A/20R-M					
	Sub-study 2.2	20A/20R-C3					
		20A/20R-C7					
		20A/20R-C28					
		20A/20R-C60					
		20A/20R-C90					

The fresh mixtures were moulded and vibrated in three prismatic samples with dimensions of 40x40x160 mm^3, and the following sequence was carried out, depending on the curing treatment:

- B: mix, stored for 24 hours at 65ºC, demolded and stored at 65ºC until the corresponding age of mechanical test.
- C: mix, stored for 48 hours at 20ºC/100% RH, demolded and stored at 20ºC/100% RH until age of mechanical test.
- M: mix, stored for 24 hours at 65ºC, demolded and stored at 20ºC/100% RH until age of mechanical test.

For the sub-studies 1.1, 1.2 and 2.1 the curing time was 7 days, and for the sub-study 2.2 the samples were tested after 3, 7, 28, 60 and 90 days.

Three values for the flexural strength (R_f) and six values for the compressive strength (R_c) were obtained according to UNE 196-1 for each mixture.

A microstructural study was carried out after 28 days of curing of the TAAMs in sub-study 2.2 (20A/20R-C28 sample) using field emission scanning electron microscopy (FESEM) and mercury intrusion porosimetry (MIP) techniques. Finally, equivalent pastes (TAAPs) were tested by thermogravimetric analysis (TGA), powder X-ray diffraction (XRD), FESEM and MIP. TGA was carried out by means of a TGA850 Mettler Toledo thermobalance instrument in N_2 atmosphere (75 $mL \cdot min^{-1}$ gas flow), with temperature range 35–500ºC and heating rate $10ºC \cdot min^{-1}$. For testing, samples of

dry paste powder (heated for 30 min at 65ºC) were placed in aluminium crucibles with sealed lids, which had a micro-hole. The mass loss and derivative curves (DTG) were obtained from the thermogravimetric curves (TG). The XRD patterns were acquired by a Bruker AXS D8 Advanced with 40 kV, 20 mA and Bragg's angle (2θ) in the 5–70º ranges. To take the FESEM images, a ZEISS Supra 55 was used, with the samples coated with carbon. An extra high tension of 20 kV and 6–8 mm of working distance were selected for the energy dispersive X-ray spectroscopy (EDS). The MIP test was carried out by means of an AutoPore IV 9500 from Micrometrics Instrument Corporation that measured pores in the 91.26 μm to 5.5 nm range.

3. Results and discussion

3.1. Step 1: OBA addition systems

3.1.1. Sub-study 1.1: Effect of OBA addition content

Three TAAMs (BFS+RHA+OBA) were prepared using different percentages of OBA addition (15, 20 and 25% by mass of BFS). The specimens were cured at 65ºC for 7 days (B curing method). As can be seen in Fig. 1.a, the specimens yielded compressive strength values that increased with the OBA percentage addition, from 15% to 25%. The mechanical behaviour for the 20A-B (20% addition) sample was 38% better than the 15A-B sample. When the percentage of OBA addition was incremented by 5% (25A-B), the compressive strength increased by only 11%. The flexural strength was 7.2 ± 0.1 MPa for 15A-B, 8.5 ± 0.2 MPa for 20A-B, and 9.2 ± 0.1 MPa for 25A-B. These values represent a progressive increment of 18% and 8%, respectively.

In a previous work, binary alkali-activated mortars (BAAMs) of BFS activated by only OBA addition were investigated and compressive strength values of 21.5 ± 0.6, 34.7 ± 1.5 and 38.4 ± 1.3 MPa for 15%, 20% and 25% respectively of OBA addition were obtained after 7 days of curing at 65ºC (de Moraes Pinheiro et al., 2018). With respect to these results, in the present work, with RHA as the silica source in the activating solution, the compressive strength increased by 77.5% in the 15% OBA addition samples, 51% in the 20% OBA addition samples and 52% in the 25% OBA addition samples. The use of RHA combined with OBA allows the dissolution of silica from the RHA, and the activation of BFS is more effective than with only OBA. The combination of 15% OBA with RHA (15A-B samples) yielded the same mechanical mortar behaviour as when only 25% OBA addition was employed (38.1 ± 0.2 MPa in TAAM with 15% OBA and 38.4 ± 1.3 MPa in BAAM) by using the same curing treatment (7 days at 65ºC).

Additionally, by comparison with the mechanical results for the binary systems obtained by de Moraes Pinheiro et al. (2018), the BAAM samples presented an increment of 61% and 10% with the 5% progressive increment of OBA addition (from 15 to 25%). The ternary samples produced in this work yielded a similar increment in the mechanical development, maintaining a constant amount of RHA, which revealed that the amount of potassium from OBA has a great influence on the BFS activated system. This behaviour could be attributed to the silica solubilisation from RHA, which is enhanced with increment of the OBA addition.

In general, the specimens in sub-study 1.1 (15A-B, 20A-B and 25A-B samples) have a very good mechanical behaviour, surpassing strengths reported for BAAMs (de Moraes Pinheiro et al. (2018). It is notable that the mechanical evolution from the 15% to 20% addition was higher than from the 20% to 25% addition. Potassium solubilisation from

OBA is more difficult as the amount of OBA increases for a fixed quantity of water. 20% OBA addition is suggested as the optimal for the TAAM system. Additionally, when 25% of OBA was employed, some difficulty was found with compacting because of poor workability. In this respect, with 5% OBA or less, the 20A-B sample yielded good characteristics in the fresh state.

3.1.2. Sub-study 1.2: Effect of curing temperature

The aim of sub-study 1.2 was to assess the effect of the curing temperature in the TAAMs previously selected (20A-B system). The curing temperature is an important factor for both BFS alkali-activated products formation and the physical and microstructural properties of the resultant materials (Fernández-Jiménez et al., 1999). The use of a high calcium precursor, such as BFS, allows a stable matrix at lower curing temperatures than the low calcium precursors (silica-alumina based precursor) (Lee and Lee, 2013).

As can be seen in Fig. 1.b, at a 65ºC curing temperature (curing method B) a higher compressive strength was reached after 7 days of curing (52.6 ± 0.4 MPa for the 20A-B sample). With the same percentage of OBA addition, when the curing treatment was carried out at 20ºC with 100% RH (curing method C, 20A-C sample), the mechanical behaviour result was 49% lower than the one observed for 20A-B. The same behaviour was observed for the flexural strength, which yielded 8.5 ± 0.2 MPa for samples cured for 7 days at 65ºC (20A-B systems) and 3.8 ± 0.3 MPa for the samples cured at 20ºC (20A-C systems). These results suggested a lower reaction rate in the short term due to the low curing temperature. The BFS activation with OBA/RHA requires a high curing temperature for fast binding gel formation with a consequent increase in strength.

The 20A-M sample (mixed curing method: 24 hours at 65ºC and 6 days at 20ºC) achieved similar mechanical behaviour to the 20A-C, reaching 2 MPa more in compressive strength when a previous 24 h treatment at 65ºC was applied (26.9 ± 0.3 MPa for 20A-C sample and 28.3 ± 0.9 MPa for 20A-M sample) and the same growth of 2 MPa for flexural strength (3.8 ± 0.3 MPa for 20A-C sample and 5.7 ± 0.9 MPa for 20A-M sample). This behaviour suggested that for good development of the binding structure, longer curing periods will be required or alternatively a high curing temperature should be used.

In a previous work reported, in which OBA was used as a potassium source, three systems were compared: BFA/H_2O, BFS/KOH (4 molar in KOH) and BFS/OBA (18% addition) (Font et al., 2017). The samples were cured at 65ºC, yielding after 3/7 days compressive strengths of 6.9 MPa/7.0 MPa, 12.7 MPa/16.9 MPa and 20.6 MPa/29.9 MPa, respectively. With the addition of just 2% more OBA and its combination with RHA for BFS activation, a significant strength increase was reached with the same curing treatment (20A-B sample).

The authors who developed alkali-activated systems with a total replacement of commercial chemical reagent obtained the following conclusions: i) Peys et al. (2016) prepared maize cob ash/MK alkali-activated systems, obtaining 30 MPa after 2 days of curing at 80ºC; ii) Van Riessen et al. (2013) used Bayer liquor for FA activation and after a mixed curing treatment (24 h at 70ºC and 27 days at room temperature) the systems yielded 43 MPa; and iii) Cheah et al. (2015) developed FA alkali-activated mortars by using wood ash (HCWA) which yielded 18 MPa after 90 days at 28ºC.

Compared with these reports, the proposed TAAMs cured at room temperature (20A-C samples) have competitive mechanical performance: the strength was lower than that

obtained after curing at 65ºC (method B). However, we assume a very good behaviour when a green material is trying to develop, avoiding the high temperature treatment (curing) which has high-energy consumptions and environmental impacts.

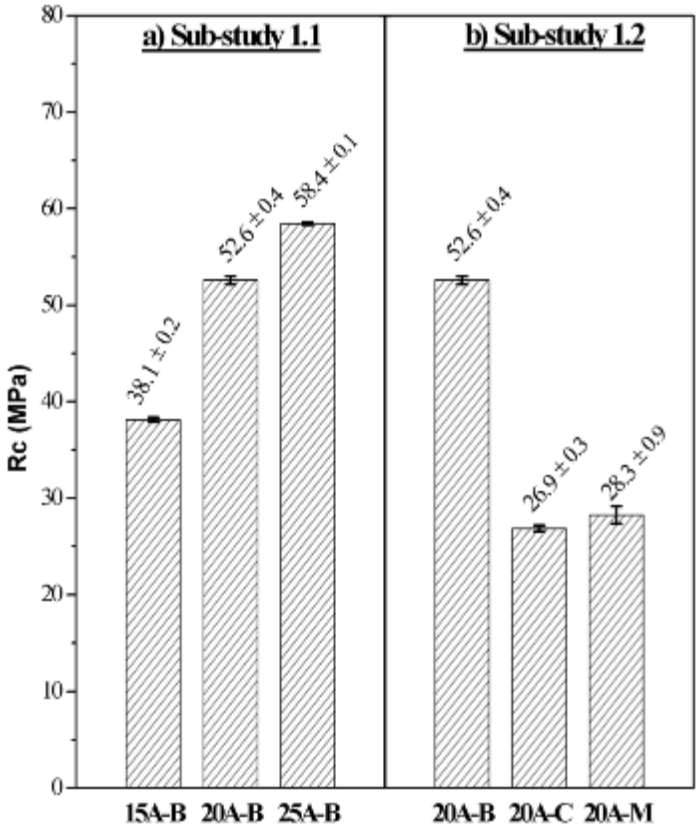

Fig. 1. Compressive strength of mortars for Step 1 after 7 days of curing: a) sub-study 1.1 (B method: curing at 65ºC); b) sub-study 1.2 (curing in different conditions; B: curing at 65ºC; C: curing at 20ºC/100% RH; and M : curing 24h method "B" + 6days method "C").

3.2. Step 2: OBA addition plus replacement systems

In order to increase the reactivity of the system, a second study (Step 2) was proposed: in this case, the OBA/BFS ratio was changed, maintaining a constant amount of RHA (see Table 2). In the previous study (Step 1, sub-study 1.2: OBA addition) the OBA/BFS ratio was 20/100, because OBA was added as 20% by mass of BFS. In this section, an additional part of the BFS was replaced (20% by mass), the OBA/BFS ratio thus being equal to 40/80. With this proposal, an increase in the alkalinity was achieved in order to enhance the solubilisation of the RHA and the reaction rate of the hydration process.

3.2.1. Sub-study 2.1: Effect of curing temperature

In this sub-study, the comparison was based on the effect of the curing temperature of the samples: methods B (65ºC, 7 days), C (20ºC, 7 days) and M (65ºC, 24 hours plus 20ºC 6 days).

The mechanical behaviour of the specimens is shown in Fig. 2.

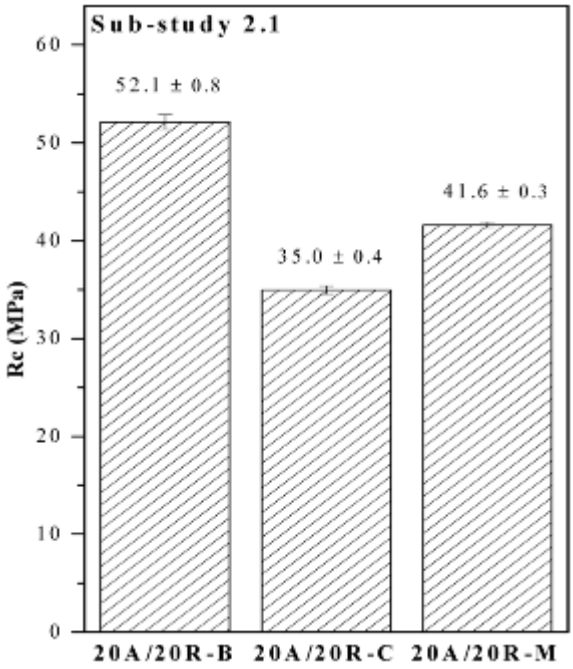

Fig. 2. Compressive strength of mortars developed in step 2: sub-study 2.1 specimens after 7 days of curing and different curing conditions.(Method B: curing at 65ºC; Method C: curing at 20ºC/100% RH; and Method M : curing 24h method "B" + 6days method "C").

The samples cured in the thermal bath at 65ºC for 7 days (20A/20R-B sample) yielded 52.1 ± 0.8 MPa of compressive strength after 7 days and, compared with the 20A-B sample (from the previous sub-study 1.2), no significant difference is observed (20A-B yielded 52.6 ± 0.4 MPa). These 20A/20R-B systems achieved 5.1 ± 0.1 MPa of flexural strength (3 MPa less than the 20A-B sample). The potassium increment from the OBA in the specimens does not have a relevant effect on the mechanical strength development when the high-temperature curing treatment is employed.

On the other hand, the mortar cured at 20ºC (20A/20R-C sample) yielded 35.0 ± 0.4 MPa of compressive strength, 23% higher with respect to the system with OBA addition (20A-C sample). This enhancement in strength is achieved with low BFS content in the mix and the better behaviour observed for the 20A/20R-C sample is attributed to the greater ability to dissolve silica from the RHA due to the higher alkalinity of the medium with respect to the 20A-C system. Qureshi and Ghosh (2013) affirmed that the compressive strength in blast furnace slag pastes cured at room temperature increases from 3 to 28 days with the increase in alkali content (%K_2O) from 4% to 8%, while keeping the water to slag ratio and silica content constant. However, the authors found a compressive strength reduction after 28 days when the K_2O percentage increased from 8% to 10%. The value of flexural strength obtained for this system was 4.6 ± 0.6 MPa, which represents an increment of 1 MPa compared with the OBA addition systems (20A-C).

Finally, for the 20A/20R-M sample, when a combined curing method was carried out (24 hours at 65°C and 6 days at 20ºC), the compressive strength was 41.6 ± 0.3 MPa, representing an increase of 45% compared with the OBA addition sample (20A-M

sample). This behaviour demonstrated that the increase in the alkalinity has an important role in the development of strength at an early age, causing an important production of cementing phase. In the case of the flexural strength, for the 20A/20R-M systems this was slightly lower than that obtained for the 20A-M sample, yielding 1.2 MPa less (4.6 ± 0.6 MPa for the 20A/20R-M).

As previously discussed in sub-study 1.2, a lower reaction rate of the geopolymerization process and the formation of the amorphous binding gel are probably influenced by the low temperature (20ºC) of the curing treatment during the early ages of the specimens. In these proposed addition/replacement series, higher silica dissolution from the RHA is possible with increase of the potassium content from the OBA.

3.2.2. Sub-study 2.2: Time evolution of strength of mortars cured at 20ºC

In the last study of the TAAM system, the time evolution of the samples cured at 20ºC/ 100% RH was assessed. The mechanical tests were carried out for the mortars after 3, 7, 28, 60 and 90 days.

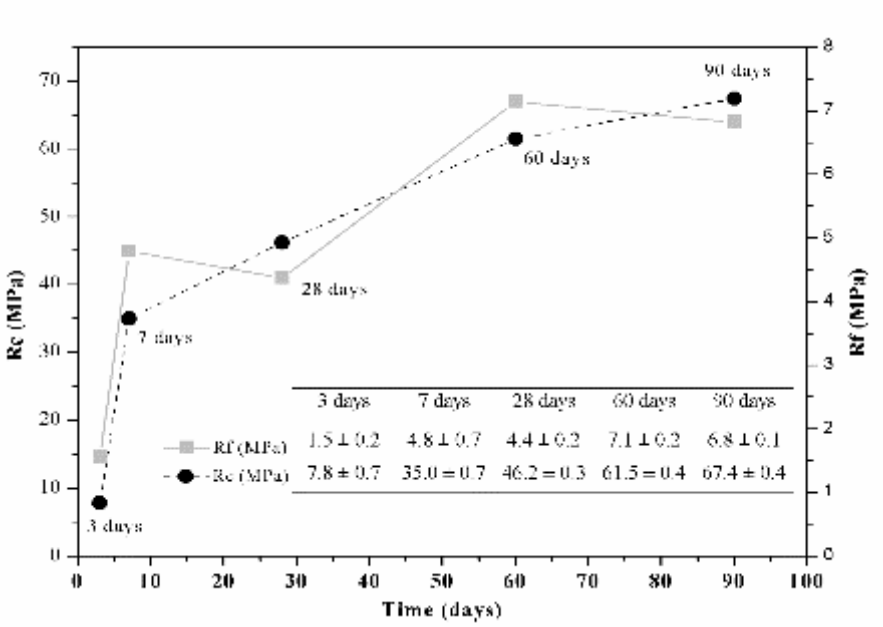

Fig. 3. Flexural (R_f) and compressive (R_c) strength development of mortars cured at 20ºC (Step 2: sub-study 2.2 specimens)

As can be seen in Fig. 3, an evident progressive increase in compressive strength from 7.8 ± 0.7 MPa to 67.4 ± 0.4 MPa was developed by the ternary system samples between 3 and 90 days respectively (approximately nine times more in strength). When geopolymers are cured at room temperature conditions, in the early curing time the precursor particles start to slowly dissolve into the activating solution. As the dissolution continues, the dissolved precursor species rearrange themselves and gradually polymerize. Consequently, by this curing treatment, the time to present a large geopolymerization is extended. Recently, Pereira et al. (2015) presented an evolution from 5.7 MPa to 46.2 MPa in compressive strength for 3 to 90 curing days in mortars based on BFS activated by KOH 8M alkali solution. The same strength evolution over time is observed when alternative alkali solutions are investigated: Luukkonen et al. (2018) presented BFS binders activated by RHA as the silica source and NaOH, obtaining a compressive strength evolution from 18 MPa at 3 days to 39/40

MPa at 90 days. BFS mortars activated by microsilica/NaOH activating solution presented a similar behaviour.

The change in the flexural strength between 3 to 90 days was 5.3 MPa. After 7 days of curing 4.8 ± 0.7 MPa were achieved. These values are slightly lower than the values obtained by de Moraes Pinheiro et al. (2018) in the BAAM (BFS activated with 20% OBA addition systems), which yielded 6.8 ± 0.6 MPa after 7 days of curing. Therefore, the value obtained in the present investigation for the TAAM was higher than those obtained by these authors in the control systems of BFS activated with KOH in 4 and 8 molar ratios (3.4 ± 0.2 MPa and 3.7 ± 0.5 MPa respectively after 7 days of curing).

From the results of the present investigation, it is possible to confirm the effectiveness of the BFS activation by using OBA (in the addition plus replacement combination) and RHA, in room temperature conditions with the curing time. The strength reached (67.4 MPa) at 90 days at 20ºC was significantly higher than that for more extreme conditions (65ºC for 7 days, 52.1 MPa), which suggested that the development of binding gel is much more effective in mild conditions. In order to confirm this point, 20A/20R-B sample was cured (three prismatic specimens) in a thermal bath at 65ºC for 14 days, finding that the compressive strength did not vary respect to 7 days curing time (49.8±1.2 MPa vs 52.1±0.8 MPa). The high-temperature curing treatment reached a limit with fast gel formation, but with the low-temperature treatment a better strength contribution of the formed gel can be observed. With the curing time, at room temperature conditions, evolution of the reaction will favour the condensation of silicates and the gel formation in the TAAM matrix and a stable material will form. This behaviour suggested that the development for long-curing ages was very favourable when room curing is carried out.

In this work it may be highlighted that after 28 days the mechanical behaviour was similar to that obtained for the TAAM cured at high temperature after 7 days in the previous sub-study 2.1 (20A/20R-B sample). Furthermore, for 20A/20R-C28 specimens the strength was 46.2 ± 0.3 MPa, a higher result than that obtained for the same curing time in previous investigations where KOH was employed as the alkaline activator and the samples required a pre-curing treatment at high temperature. Thus, Tippayasam et al. (2016) recently presented metakaolin-based geopolymers activated by 10M KOH and a K_2SiO_3/KOH mass ratio of 1.5 that yielded 30.3 MPa after 24 h at 40ºC and 27 days at 25ºC. The BFS-based mortars activated by using KOH reagent in 8M yielded 35.5 MPa after 24 h at 25ºC, 7 h at 65ºC and storage at room temperature until 28 days (Pereira et al., 2015). The use of RHA as an alternative silica source mixed with NaOH for the activation of BFS-based geopolymers was carried out by Moraes et al. (2018) obtaining 59.7 MPa after 28 curing days at 20ºC. The investigation showed values of 54.9 MPa when SCSA was employed as a silica source under the same conditions. All these comparisons show that the activation of BFS by a mixture of OBA and RHA led to very good mechanical performance for the medium and long terms.

3.3. Microstructural characterization of TAAMs

XRD patterns of the TAAPs from sub-study 2.2 (pastes) are presented in Fig. 4. A baseline deviation of the Bragg's angle in the range from 25º to 40° was observed in all cases. This baseline deviation is characteristic of geopolymerized BFS pastes, as was shown by several authors (Moraes et al., 2017; Pereira et al., 2015), and it is attributed to the gel formation. The same characteristic peaks for 20A/20R-C pastes were identified for all analyzed curing ages. The main crystalline peaks of calcite ($CaCO_3$, PDFcard 050586), quartz (SiO_2, PDFcard 331161) and hydrotalcite

($Mg_6Al_2CO_3(OH)_{16}$, PDFcard 411428) were observed. Additionally, some minor peaks corresponding to arcanite (K_2SO_4, PDFcard 050613), hydroxyapatite ($Ca_5(PO_4)_3(OH)$, PDFcard 090432) and cristobalite (SiO_2, PDFcard 391425) were identified. Seeing the chemical composition of the raw materials (Table 1), it is possible to deduce that the presence of calcite as well as the crystalline quartz phases suggest the unreacted BFS and OBA particles and is probably because it did not react in the activating process (Moraes et al., 2017). Beltrán et al. (2016) identified the peaks of arcanite in the XRD spectrum of the biomass bottom ash from the olive pruning waste after combustion at 403ºC. The presence of arcanite may be attributed to a combination of some OBA compounds: K_2O (32.12% by weight) and SO_3 (1.67% by weight). When the BFS has more than 5% by weight of MgO, the hydrotalcite peak is commonly observed as a part of the main reaction products (Adesanya et al., 2018). Thus, as is shown in Table 1, the BFS used in the present investigation has 7.43% by weight of MgO. The hydrotalcite was previously identified in pastes of BFS activated with OBA by Font et al. (2017). Finally the cristobalite peaks can be attributed to the RHA (Luukkonen et al., 2018).

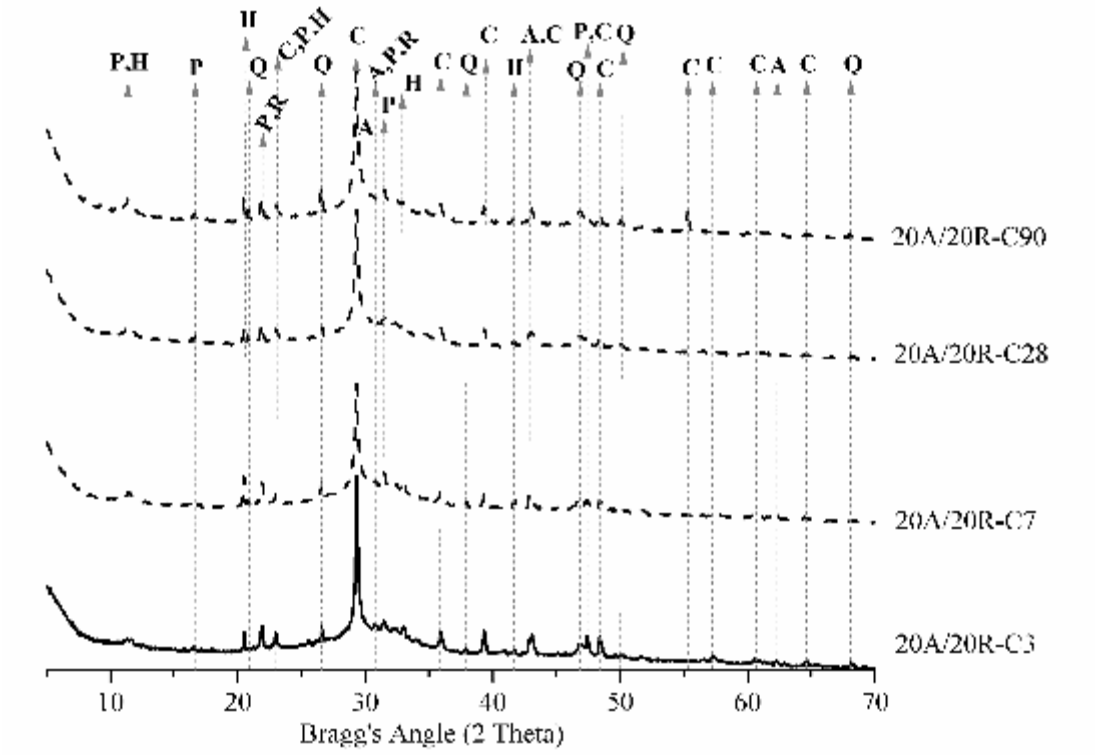

Fig. 4. XRD patterns of TAAPs from sub-study 2.2 (Key: Q = quartz; R = cristobalite; C = calcite; A = arcanite; P = hydroxyapatite; H = hydrotalcite).

Derivate thermogravimetric curves (DTG) for the TAAPs from sub-study 2.2 are shown in Fig. 5. The literature shows DTG analysis for BFS pastes with the distribution of mass losses in characteristic peaks which appear in the following temperature ranges: i) between 110–140ºC corresponding to the loss of combined water from the main hydrated products C-S-H and (C-x)-S-H (with x = Na (in sodium-activated systems) or K (in potassium-activated systems)); ii) between 140–200ºC related to the dehydration of (C-x)-A-S-H (normally in the range between 140–155ºC) and C-A-S-H (in the range from 180 to 200ºC); and iii) at about 390ºC, which is commonly related with the

dehydration of hydrotalcite (de Moraes Pinheiro et al., 2018; Moraes et al., 2018; Rivera et al., 2016). The thermogravimetric analysis carried out by Font et al. (2017)showed the first two characteristic peaks in pastes of BFS/water related to i) and ii) above-mentioned mass losses and the presence of the DTG peak related to the hydrotalcite in pastes of BFS/KOH 4M and BFS/OBA (18% addition). Pereira et al. (2015) found only one characteristic peak between 145–170ºC in BFS pastes activated by NaOH solution, corresponding to dehydration of the reaction gels formed.

In the DTG curves obtained for the TAAPs, it can be noticed that a very similar DTG characteristic peak was found when comparing the curves (Fig. 5). In general terms, the DTG curves for the TAAPs showed only one large DTG peak at the temperature range between 128–140ºC. The mass losses corresponding to the different decomposition/dehydration of C-A-S-H and (C-K)-A-S-H were produced together in the same temperature range. These results may be due to the formation of gels with a different nature yielding a stronger matrix by the addition of a silica source in the system (from RHA) and its combination with a higher amount of potassium and calcium from OBA. Although the corresponding hydrotalcite peak was identified in the XRD patterns of the pastes, in the DTG curves it was difficult to observe: a small deviation was perceived in the range 380–420ºC.

Furthermore, as indicated in Fig. 5, the total mass losses (35–500ºC) increased from 3 to 90 days of curing, suggesting that the quantity of hydrated compounds was increasing during the curing of the pastes.

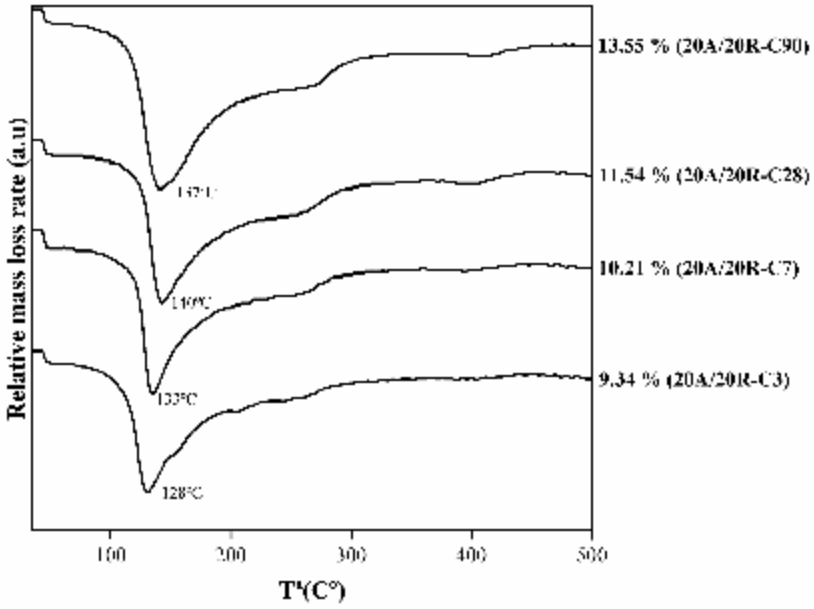

Fig. 5. DTG curves of TAAPs from sub-study 2.2 (20ºC curing). Percentages on the right indicate the total mass loss in the 35–500ºC range.

By comparing the results of the total mass losses from the TGA and the TAAMs mechanical behaviour discussed above (Fig. 3) in sub-study 2.2, a sample evolution with age can be observed in both cases: mass loss as well as compressive strength

increased with curing time. With the progress of the BFS alkaline activation, more hydrated products are formed and consequently the mortars developed better compressive strength behaviour. Between 3 and 90 days there is an increase of ≈ 88.5% in compressive strength and ≈ 30.8% in total mass loss. A linear relationship between the compressive strength and the mass loss was obtained (Fig. 6).

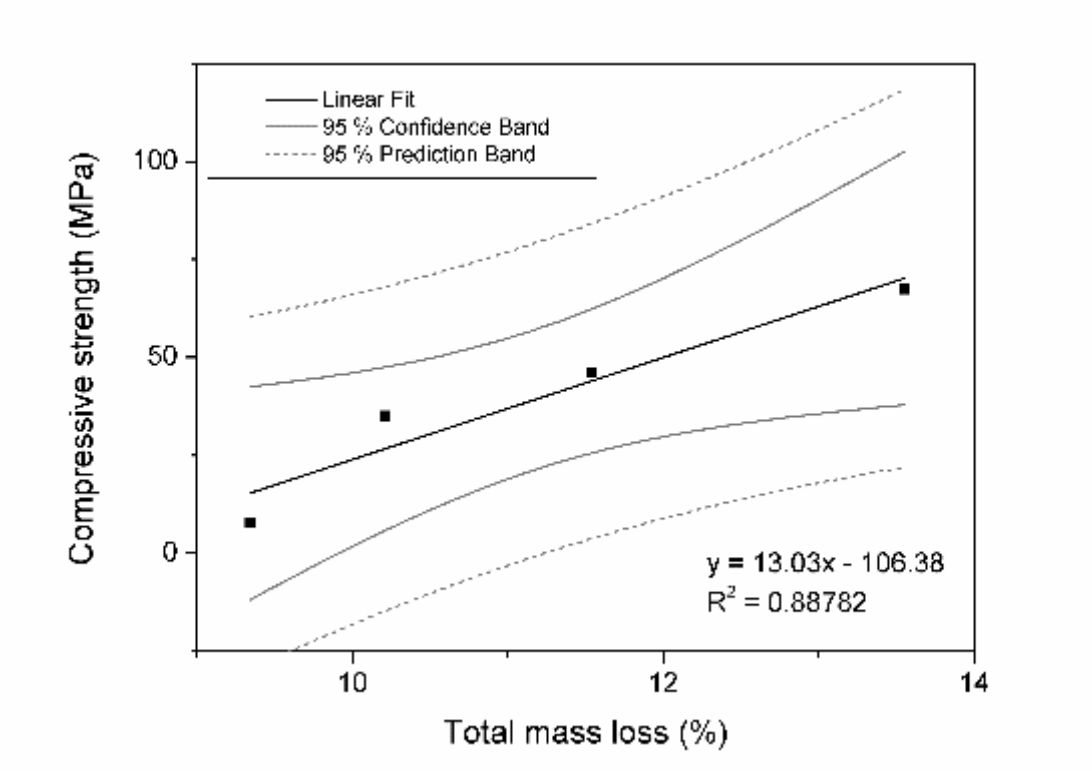

Fig. 6. Linear fit model between compressive strength and thermogravimetric mass loss for 20A/20R-C sample (curing ages: 3, 7, 28 and 90 days).

A similar linear relationship between the compressive strength and the thermogravimetric mass loss with the curing time was obtained by Moraes et al. (2018) in pastes of BFS and BFS with SCSA in 25% replacement, activated by NaOH or NaOH/commercial waterglass solutions. The results obtained for 20A/20R-C pastes suggested that, with the OBA/RHA blending for BFS activation, it is possible to obtain the synthesis of the traditional gel forms for slag.

The MIP curves of the 20A/20R TAAM and TAAP cured for 28 days are shown in Fig. 7, where the accumulated distribution of the intruded Hg volume per gram of material is represented as a function of the pore size diameter. Inserted in these graphs are tables with the porosimetry parameters obtained for TAAM and TAAP of 20/20R-C28 samples. In the curves, vertical lines mark the pore structure differentiation into gel pores, capillary pores and air voids, according to the authors (Aligizaki, 2006; Neville, 1982) .

For the TAAM sample, the total porosity was 12.48%, of which 40.60% correspond to gel pores, 56.65% correspond to capillary pores and the remaining 2.75% correspond to air voids. In the case of the paste (TAAP), as expected, the total porosity was higher than the mortar one (21.22%) due to the absence of sand in the sample, and consequently the volume of paste analysed was higher. In the TAAP sample, 39.00% of the porosity corresponds to the gel pores, 59.88% to the capillary pores and 1.12%

to the air voids. It can be seen that the proportions of the different kinds of pores for mortar and paste were equivalent. de Moraes Pinheiro et al. (2018) affirmed that the increment of the OBA addition in the BFS pastes causes a reduction of total porosity, which was correlated with the compressive strength increment in mortars. The pastes based on BFS/OBA systems resulted in a total porosity of 42.85% when 10% of OBA was added and of 29.16% when 25% of OBA was added. In the present work the TAAP resulted in a lower total porosity because of the higher total OBA employed (40%, which is equivalent to 20% addition plus 20% substitution) and the chemical effect of RHA dissolution and reaction towards BFS.

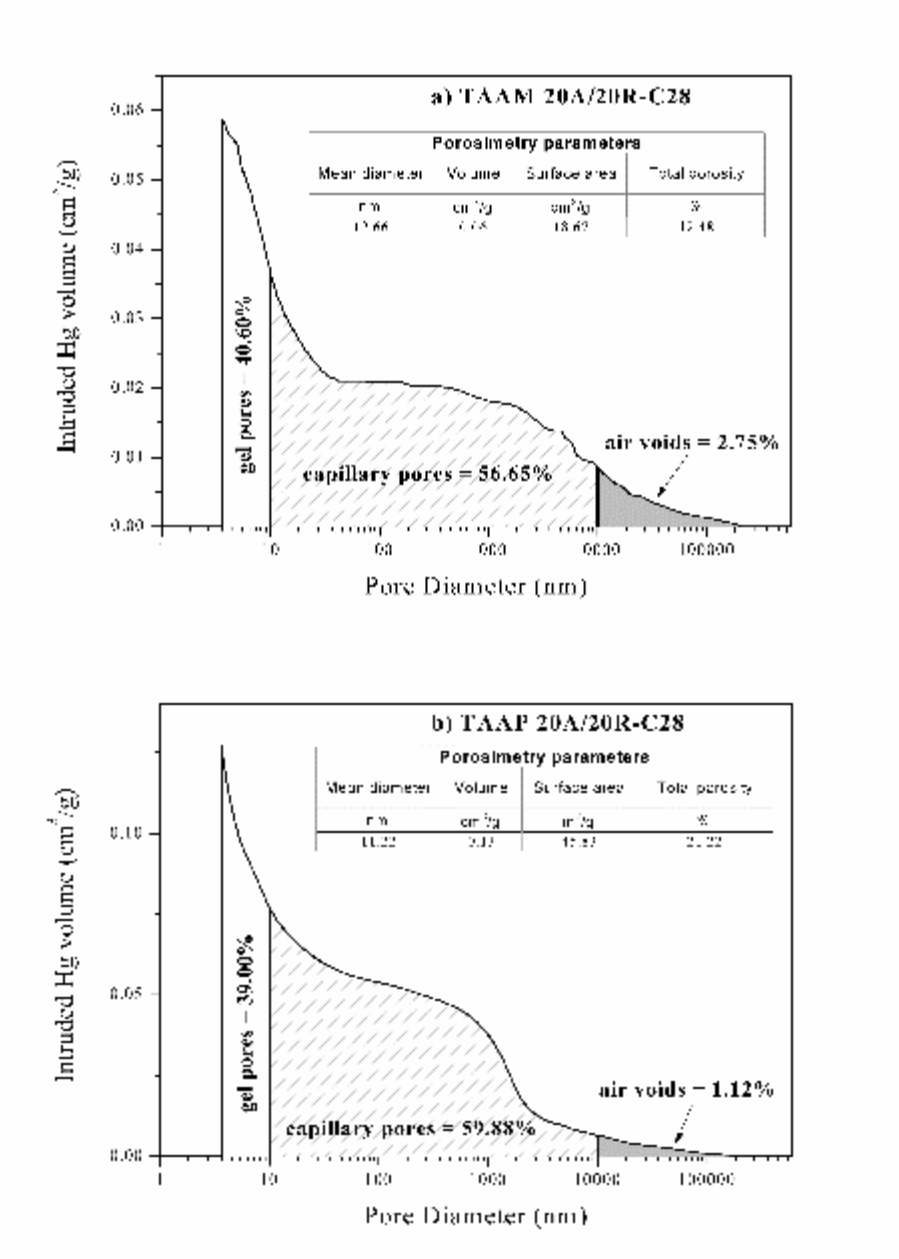

Fig. 7. Results from MIP for: a) 20A/20R-C28 mortar (TAAM); b) 20A/20R-C28 paste (TAAP).

FESEM micrographs of the TAAP after 28 days at 20ºC (20A/20R-C28 sample) are shown in Figs. 8 and 9. In the selected micrographs the most representative topography and gel particles and their details can be observed. As can be appreciated, the paste matrix presented three different particle morphologies in terms of shape.

The first micrograph (Fig. 8a) shows an overview of the paste surface with a dense and compact topography without large pores. In the previous investigation of binary pastes based on BFS/OBA, a highly porous surface was observed (de Moraes Pinheiro et al., 2018). The incorporation of RHA in the ternary systems allows the reduction of the matrix micro-porosity by the silicates reaction forming inter-clustered gels. Two main structures can be distinguished in this micrograph as shown in Figs 8b and 8c:

i) A particle of BFS appears in the centre of Fig. 8a and the first detail shown in Fig. 8b corresponds to hydration products (0.1–0.5 µm in size) formed on the BFS particles. The EDS analysis yielded MgO = 3.1 ± 1.3%, Al_2O_3 = 5.3 ± 1.7%, SiO_2 = 16.1 ± 3.8%, K_2O = 20.1 ± 4.7% and CaO = 53.1 ± 6.3% as principal oxides. The presence of MgO can be attributed to the BFS. The gel can be identified as C(K)-S(A)-H.

ii) The second detail of the micrograph (Fig. 8c) corresponds to a different crystallization pattern where the matrix is less dense than the other zone (Fig. 8b) and no magnesium or aluminium were in the chemical composition determined by EDS. The EDS analysis of the zone yielded a lower amount of silica (6.2 ± 0.9%) and CaO (42.9 ± 3.3%) and a higher amount of K_2O (48.3 ± 3.5%). The gel can be labelled as C(K)-S-H. A similar morphology of the particles was found by de Moraes Pinheiro et al. (2018) in pastes of BFS/OBA binary systems.

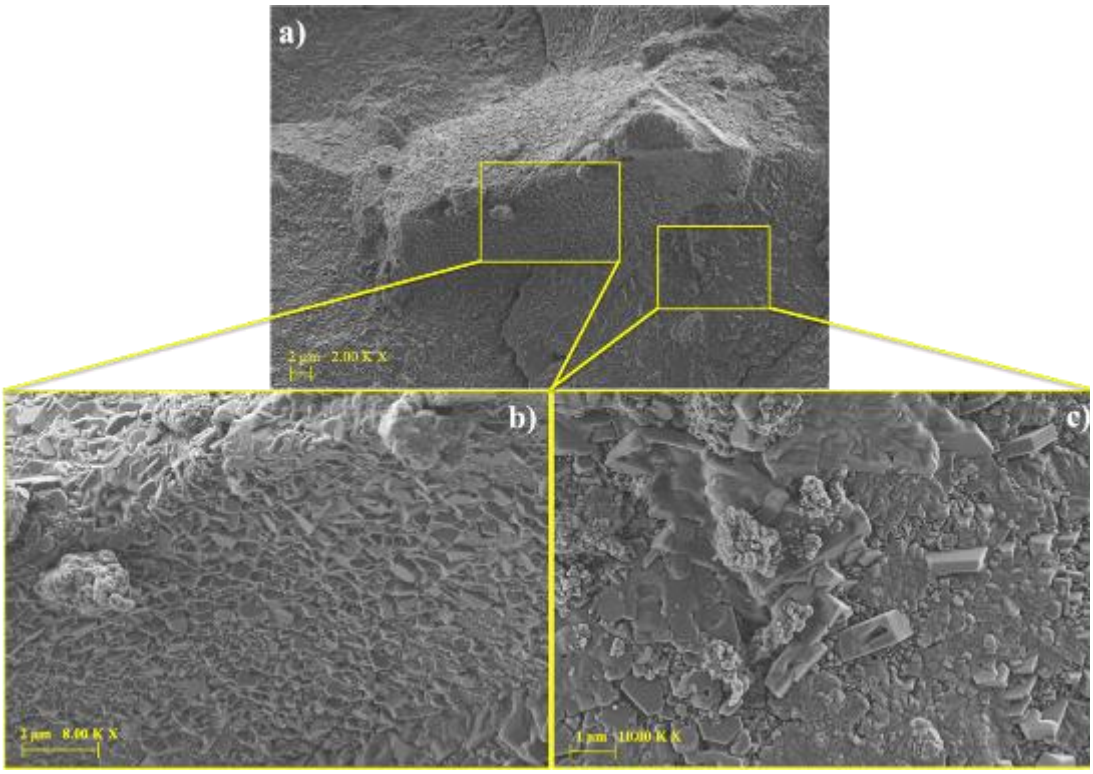

Fig. 8. FESEM micrographs of pastes from sub-study 2.2 samples cured for 28 days at 20ºC (20A/20R-C28 paste): a) general view in 2000x magnification; b) detail of the one characteristic zone from the above micrograph in 8000x magnification; and

c) detail of the other characteristic zone from micrograph a) in 10000x magnification.

In the other micrograph (Fig. 9) thinner and more isolated microcrystals can be observed in the dense matrix of the material. These microcrystals have flat flake morphology, as shown in the detail of the zone where they are located (Fig. 9b). In other investigations, these characteristic formations were attributed to the formation of Mg-Al-CO_3-hydrotalcite microcrystals (Liao et al., 2012). As discussed above, in the XRD section, the patterns of the 20A/20R-C28 paste presented hydrotalcite peaks.

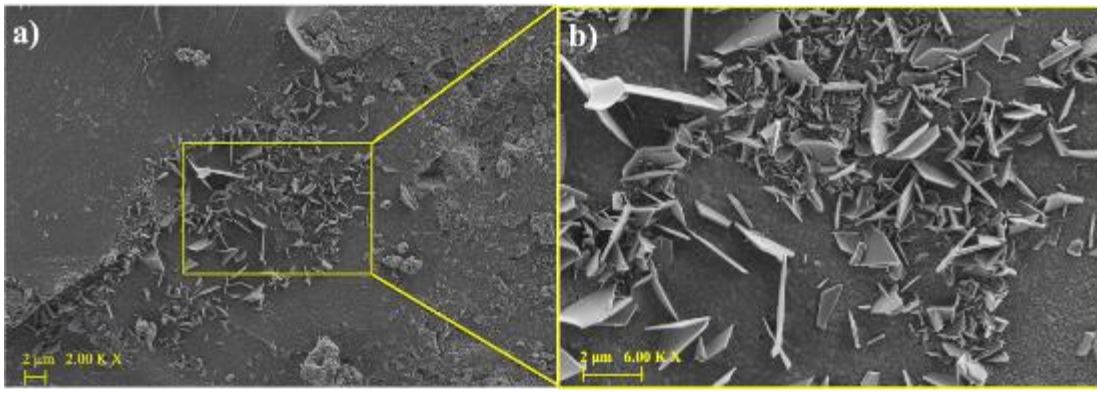

Fig. 9. FESEM micrographs of pastes from sub-study 2.2 samples cured for 28 days at 20ºC (20A/20R-C28 paste): a) general view in 2000x magnification; b) detail of the microcrystals from the above micrograph in 6000x magnification.

4. Conclusions

The main conclusion from the present investigation is the successful development of new ternary alkali-activated systems that are 100% waste based on: blast furnace slag (BFS), olive-stone biomass ash (OBA) and rice husk ash (RHA).

Respect the mechanical test on TAAMs, the following statements can be done:

- The ternary alkali-activated mortars (TAAM), where the OBA/BFS ratio was changed while keeping the amount of RHA constant, showed an enhanced strength development when the OBA proportion in the BFS weight addition was increased from 15% to 25%.
- Focusing the study on the TAAMs' behaviour with respect to different curing conditions, the high temperature (65ºC) produced a fast reaction in the binder gel formation. The combined curing method (65ºC for 24 hours plus 20ºC for 6 days) does not produce remarkable differences in the mechanical behaviour of the TAAMs. A 20ºC curing temperature produced the hydration products gently and consequently the mechanical strength development is slower.
- The use of OBA as addition plus the replacement of BFS by OBA (where the OBA/BFS ratio was increased from 0.25 to 0.5) made it possible to obtain excellent strength development, especially for mortars cured at 20ºC. For the TAAMs with 0.5 OBA/BFS ratio, very good performance of the mortars was produced after 28 and 90 days of curing: 46 and 67 MPa were

reached respectively. It is highlighted that these values were significantly better than those previously obtained for binary alkali-activated systems of BFS/OBA, suggesting that the RHA has an important role in the development of these alternative materials.

From the microstructural characterization of BFS/OBA/RHA system with 0.5 OBA/BFS ratio, the following is concluded:

- The reaction of the OBA with the RHA dissolved part of the potassium and the silica, forming potassium silicate. This potassium silicate enhanced the alkali activation of the BFS. The microstructural results demonstrated that a large amount of gel was formed during the curing of the ternary BFS/OBA/RHA system.
- In XRD patterns of the ternary pastes (TAAP), the main crystalline peaks of calcite, quartz and hydrotalcite were identified and some minor peaks corresponding to arcanite, hydroxyapatite and cristobalite were also identified.
- The DTG curves showed a large peak corresponding to the decomposition/dehydration of C(K)-S-H and (C(K)-S(A)-H gels together. The combination of silica from RHA and potassium from OBA allows a strong gel matrix development.
- The corresponding hydrotalcite peak identified in the XRD patterns was difficult to observe in DTG curves.
- For TAAM, the total porosity was 12.48 % and for TAAP was 21.22 %. The main type of pores found in both samples (TAAM and TAAP) was the capillary pore.
- The FESEM micrographs showed an important dense matrix with the presence of two types of microcrystals. The EDS results demonstrated that a large amount of gel was formed during the curing of the ternary pastes. Two types of gel were identified, one of them containing mainly Ca/K/Si/Al (C(K)-S(A)-H gel) and the other containing Ca/K/Si (C(K)-S-H gel).

As final conclusion, the mixing of OBA and RHA is an interesting proposal for increasing the alkali activation rate of BFS.

Conflict of interest

None.

Acknowledgements

The authors gratefully acknowledge the GeocelPlus-UPV project, Almazara Candela – Elche, Spain and DACSA S.A. - Tabernes Blanques, Spain. Thanks are also given to the Electron Microscopy Service of the Universitat Politècnica de València.

References

Adesanya, E., Ohenoja, K., Luukkonen, T., Kinnunen, P., Illikainen, M., 2018. One-part geopolymer cement from slag and pretreated paper sludge. J. Clean. Prod. https://doi.org/10.1016/j.jclepro.2018.03.007

Aligizaki, K.K., 2006. Pore structure of cement-based materials, First. ed. Taylor &

Francis, Canada and USA.

Andrew, R.M., 2018. Global CO 2 emissions from cement production. Earth Syst. Sci. Data 10, 2213–2239.

Beltrán, M.G., Barbudo, A., Agrela, F., Jiménez, J.R., De Brito, J., 2016. Mechanical performance of bedding mortars made with olive biomass bottom ash. Constr. Build. Mater. https://doi.org/10.1016/j.conbuildmat.2016.02.065

Bernal, S.A., Rodríguez, E.D., Mejía de Gutiérrez, R., Provis, J.L., 2015. Performance at high temperature of alkali-activated slag pastes produced with silica fume and rice husk ash based activators. Mater. Construcción 65, e049. https://doi.org/10.3989/mc.2015.03114

Bouzón, N., Payá, J., Borrachero, M. V., Soriano, L., Tashima, M.M., Monzó, J., 2014. Refluxed rice husk ash/NaOH suspension for preparing alkali activated binders. Mater. Lett. 115, 72–74. https://doi.org/10.1016/j.matlet.2013.10.001

Cheah, C.B., Part, W.K., Ramli, M., 2015. The hybridizations of coal fly ash and wood ash for the fabrication of low alkalinity geopolymer load bearing block cured at ambient temperature. Constr. Build. Mater. 88, 41–55. https://doi.org/10.1016/j.conbuildmat.2015.04.020

de Moraes Pinheiro, S.M., Font, A., Soriano, L., Tashima, M.M., Monzó, J., Borrachero, M.V., Payá, J., 2018. Olive-stone biomass ash (OBA): An alternative alkaline source for the blast furnace slag activation. Constr. Build. Mater. https://doi.org/10.1016/j.conbuildmat.2018.05.157

Fernández-Jiménez, A., Cristelo, N., Miranda, T., Palomo, Á., 2017. Sustainable alkali activated materials: Precursor and activator derived from industrial wastes. J. Clean. Prod. 162, 1200–1209. https://doi.org/10.1016/j.jclepro.2017.06.151

Fernández-Jiménez, A., Palomo, J.G., Puertas, F., 1999. Alkali-activated slag mortars: Mechanical strength behaviour. Cem. Concr. Res. https://doi.org/10.1016/S0008-8846(99)00154-4

Font, A., Soriano, L., Moraes, J.C.B., Tashima, M.M., Monzó, J., Borrachero, M.V., Payá, J., 2017. A 100% waste-based alkali-activated material by using olive-stone biomass ash (OBA) and blast furnace slag (BFS). Mater. Lett. 203. https://doi.org/10.1016/j.matlet.2017.05.129

Font, A., Soriano, L., Reig, L., Tashima, M.M., Borrachero, M. V, Monzó, J., Payá, J., 2018. Use of residual diatomaceous earth as a silica source in geopolymer production. Mater. Lett. 223, 10–13. https://doi.org/10.1016/j.matlet.2018.04.010

Hu, W., Nie, Q., Huang, B., Shu, X., He, Q., 2018. Mechanical and microstructural characterization of geopolymers derived from red mud and fly ashes. J. Clean. Prod. 186, 799–806. https://doi.org/10.1016/j.jclepro.2018.03.086

Lee, N.K., Lee, H.K., 2013. Setting and mechanical properties of alkali-activated fly ash/slag concrete manufactured at room temperature. Constr. Build. Mater. https://doi.org/10.1016/j.conbuildmat.2013.05.107

Liao, L., Zhao, N., Xia, Z., 2012. Hydrothermal synthesis of Mg-Al layered double hydroxides (LDHs) from natural brucite and Al(OH) 3. Mater. Res. Bull. 47, 3897–3901. https://doi.org/10.1016/j.materresbull.2012.07.007

Luukkonen, T., Abdollahnejad, Z., Yliniemi, J., Kinnunen, P., Illikainen, M., 2018.

638 Comparison of alkali and silica sources in one-part alkali-activated blast furnace
639 slag mortar. J. Clean. Prod. 187, 171–179.
640 https://doi.org/10.1016/j.jclepro.2018.03.202

641 Mejía, J.M., Mejía De Gutiérrez, R., Montes, C., 2016. Rice husk ash and spent
642 diatomaceous earth as a source of silica to fabricate a geopolymeric binary
643 binder. J. Clean. Prod. 118, 133–139.
644 https://doi.org/10.1016/j.jclepro.2016.01.057

645 Mejía, J.M., Mejía de Gutiérrez, R., Puertas, F., 2013. Ceniza de cascarilla de arroz
646 como fuente de sílice en sistemas cementicios de ceniza volante y escoria
647 activados alcalinamente. Mater. Construcción 63, 361–375.
648 https://doi.org/10.3989/mc.2013.04712

649 Mellado, A., Catalán, C., Bouzón, N., Borrachero, M. V., Monzó, J.M., Payá, J.,
650 2014. Carbon footprint of geopolymeric mortar: study of the contribution of the
651 alkaline activating solution and assessment of an alternative route. RSC Adv. 4,
652 23846–23852. https://doi.org/10.1039/C4RA03375B

653 Moraes, J.C.B., Font, A., Soriano, L., Akasaki, J.L., Tashima, M.M., Monzó, J.,
654 Borrachero, M.V., Payá, J., 2018. New use of sugar cane straw ash in alkali-
655 activated materials: A silica source for the preparation of the alkaline activator.
656 Constr. Build. Mater. 171. https://doi.org/10.1016/j.conbuildmat.2018.03.230

657 Moraes, J.C.B., Tashima, M.M., Akasaki, J.L., Melges, J.L.P., Monzó, J., Borrachero,
658 M. V., Soriano, L., Payá, J., 2017. Effect of sugar cane straw ash (SCSA) as
659 solid precursor and the alkaline activator composition on alkali-activated binders
660 based on blast furnace slag (BFS). Constr. Build. Mater. 144, 214–224.
661 https://doi.org/10.1016/j.conbuildmat.2017.03.166

662 Neville, A.M., 1982. Properties of concrete, Fifth. ed. Pearson Education Limited,
663 England.

664 Nie, Q., Hu, W., Huang, B., Shu, X., He, Q., 2019. Synergistic utilization of red mud
665 for flue-gas desulfurization and fly ash-based geopolymer preparation. J. Hazard.
666 Mater. 369, 503–511. https://doi.org/10.1016/j.jhazmat.2019.02.059

667 Passuello, A., Rodríguez, E.D., Hirt, E., Longhi, M., Bernal, S.A., Provis, J.L.,
668 Kirchheim, A.P., 2017. Evaluation of the potential improvement in the
669 environmental footprint of geopolymers using waste-derived activators. J. Clean.
670 Prod. 166, 680–689. https://doi.org/10.1016/j.jclepro.2017.08.007

671 Payá, J., Monzó, J., Borrachero, M.V., Soriano, L., Akasaki, J.L., Tashima, M.M.,
672 2017. New inorganic binders containing ashes from agricultural wastes,
673 Sustainable and Nonconventional Construction Materials using Inorganic
674 Bonded Fiber Composites. https://doi.org/10.1016/B978-0-08-102001-2.00006-1

675 Pereira, A., Akasaki, J.L., Melges, J.L.P., Tashima, M.M., Soriano, L., Borrachero,
676 M. V., Monzó, J., Payá, J., 2015. Mechanical and durability properties of alkali-
677 activated mortar based on sugarcane bagasse ash and blast furnace slag. Ceram.
678 Int. 41, 13012–13024. https://doi.org/10.1016/j.ceramint.2015.07.001

679 Peys, A., Rahier, H., Pontikes, Y., 2016. Potassium-rich biomass ashes as activators
680 in metakaolin-based inorganic polymers. Appl. Clay Sci.
681 https://doi.org/10.1016/j.clay.2015.11.003

682 Qureshi, M.N., Ghosh, S., 2013. Effect of Alkali Content on Strength and

683 Microstructure of GGBFS Paste. Glob. J. Res. Eng. Civ. Struct. Eng. 13, 11–20.

684 Rivera, O.G., Long, W.R., Weiss, C.A., Moser, R.D., Williams, B.A., Torres-Cancel,
685 K., Gore, E.R., Allison, P.G., 2016. Effect of elevated temperature on alkali-
686 activated geopolymeric binders compared to portland cement-based binders.
687 Cem. Concr. Res. 90, 43–51. https://doi.org/10.1016/j.cemconres.2016.09.013

688 Shirley, R., Black, L., 2011. Alkali activated solidification/stabilisation of air
689 pollution control residues and co-fired pulverised fuel ash. J. Hazard. Mater. 194,
690 232–242. https://doi.org/10.1016/j.jhazmat.2011.07.100

691 Tchakouté, H.K., Rüscher, C.H., Kong, S., Kamseu, E., Leonelli, C., 2016.
692 Geopolymer binders from metakaolin using sodium waterglass from waste glass
693 and rice husk ash as alternative activators: A comparative study. Constr. Build.
694 Mater. 114, 276–289. https://doi.org/10.1016/j.conbuildmat.2016.03.184

695 Tippayasam, C., Balyore, P., Thavorniti, P., Kamseu, E., Leonelli, C., Chindaprasirt,
696 P., Chaysuwan, D., 2016. Potassium alkali concentration and heat treatment
697 affected metakaolin-based geopolymer. Constr. Build. Mater.
698 https://doi.org/10.1016/j.conbuildmat.2015.11.027

699 Torres-Carrasco, M., Puertas, F., 2015. Waste glass in the geopolymer preparation.
700 Mechanical and microstructural characterisation. J. Clean. Prod. 90, 397–408.
701 https://doi.org/10.1016/j.jclepro.2014.11.074

702 Turner, L.K., Collins, F.G., 2013. Carbon dioxide equivalent (CO2-e) emissions: A
703 comparison between geopolymer and OPC cement concrete. Constr. Build.
704 Mater. 43, 125–130. https://doi.org/10.1016/j.conbuildmat.2013.01.023

705 Van Riessen, A., Jamieson, E., Kealley, C.S., Hart, R.D., Williams, R.P., 2013.
706 Bayer-geopolymers: An exploration of synergy between the alumina and
707 geopolymer industries. Cem. Concr. Compos. 41, 29–33.
708 https://doi.org/10.1016/j.cemconcomp.2013.04.010

709 Wang, S.-D., Pu, X.-C., Scrivener, K.L., Pratt, P.L., 1995. Alkali-activated slag
710 cement and concrete: a review of properties and problems. Adv. Cem. Res. 7,
711 93–102. https://doi.org/10.1680/adcr.1995.7.27.93

712 World busines council for sustainable development [WWW Document], n.d. URL
713 https://www.wbcsd.org/Sector-Projects/Cement-Sustainability-
714 Initiative/News/Cement-technology-roadmap-shows-how-the-path-to-achieve-
715 CO2-reductions-up-to-24-by-2050 (accessed 6.11.19).

716 Yang, K.H., Song, J.K., Song, K. Il, 2013. Assessment of CO 2 reduction of alkali-
717 activated concrete. J. Clean. Prod. 39, 265–272.
718 https://doi.org/10.1016/j.jclepro.2012.08.001

719